

Modeling the Impact of Wind Intensification on Antarctic Sea Ice Volume

JINLUN ZHANG

Polar Science Center, Applied Physics Laboratory, University of Washington, Seattle, Washington

(Manuscript received 5 March 2012, in final form 15 June 2013)

ABSTRACT


A global sea ice–ocean model is used to examine the impact of wind intensification on Antarctic sea ice volume. Based on the NCEP–NCAR reanalysis data, there are increases in surface wind speed ($0.13\% \text{ yr}^{-1}$) and convergence ($0.66\% \text{ yr}^{-1}$) over the ice-covered areas of the Southern Ocean during the period 1979–2010. Driven by the intensifying winds, the model simulates an increase in sea ice speed, convergence, and shear deformation rate, which produces an increase in ridge ice production in the Southern Ocean ($1.1\% \text{ yr}^{-1}$). The increased ridged ice production is mostly in the Weddell, Bellingshausen, Amundsen, and Ross Seas where an increase in wind convergence dominates. The increase in ridging production contributes to an increase in the volume of thick ice (thickness $> 2 \text{ m}$) in the Southern Ocean, while the volumes of thin ice (thickness $\leq 1 \text{ m}$) and medium thick ice ($1 \text{ m} < \text{thickness} \leq 2 \text{ m}$) remain unchanged over the period 1979–2010. The increase in thick ice leads to an increase in ice volume in the Southern Ocean, particularly in the southern Weddell Sea where a significant increase in ice concentration is observed. The simulated increase in either the thick ice volume ($0.91\% \text{ yr}^{-1}$) or total ice volume ($0.46\% \text{ yr}^{-1}$) is significantly greater than other ice parameters (simulated or observed) such as ice extent ($0.14\text{--}0.21\% \text{ yr}^{-1}$) or ice area fraction ($0.24\%\text{--}0.28\% \text{ yr}^{-1}$), suggesting that ice volume is a potentially strong measure of change.

1. Introduction

Climate changes observed in the Antarctic include the significant poleward intensification of the westerly winds over the Southern Ocean (SO) since the 1970s (Hurrell and van Loon 1994; Thompson and Solomon 2002). The intensification of the westerly winds is closely linked to the southern annular mode (SAM), which represents a dominant mode of atmospheric variability in the Southern Hemisphere. Over the past decades, the SAM has shifted to more positive phases, as reflected in a general increase in the SAM index (e.g., Kidson 1999; Marshall 2003). Such a shift is associated with a strengthening of the circumpolar vortex and hence the intensification of the westerly winds in the SO. The observation of poleward intensification of the westerly winds is consistent with global climate model simulations of increasing SO surface winds in the twentieth and twenty-first centuries (Fyfe and Saenko 2006).

Simulations of Antarctic sea ice are reported to be sensitive to surface wind forcing. The intensification of SO surface winds affects Antarctic sea ice in some model experiments (e.g., Hall and Visbeck 2002; Spence et al. 2010). Sea ice coverage tends to expand with intensifying winds and concurrent ocean circulation changes in an unforced 15 000-yr integration of a global climate model that allows ice to move following ocean currents without incorporating ice dynamics (Hall and Visbeck 2002). Sea ice tends to decline to a varying degree, depending on model resolution, with intensifying winds in future climate warming scenarios according to a global climate model that includes dynamic and thermodynamic sea ice components (Spence et al. 2010). However, few model studies have focused on the impact of the observed SO wind intensification on Antarctic sea ice in the past decades when satellite passive microwave images show a modest increase in the Antarctic sea ice cover (e.g., Parkinson and Cavalieri 2012).

This model study explores the effect of changes in winds on the variability and trends of Antarctic sea ice during the period 1979–2010. The focus of this study is on the impact of wind intensification on changes in sea ice volume. Linked to the energy balance of the Antarctic climate system, Antarctic sea ice volume is a useful

 Denotes Open Access content.

Corresponding author address: Jinlun Zhang, Polar Science Center, Applied Physics Laboratory, University of Washington, 1013 NE 40th St., Seattle, WA 98105.
E-mail: zhang@apl.washington.edu

DOI: 10.1175/JCLI-D-12-00139.1

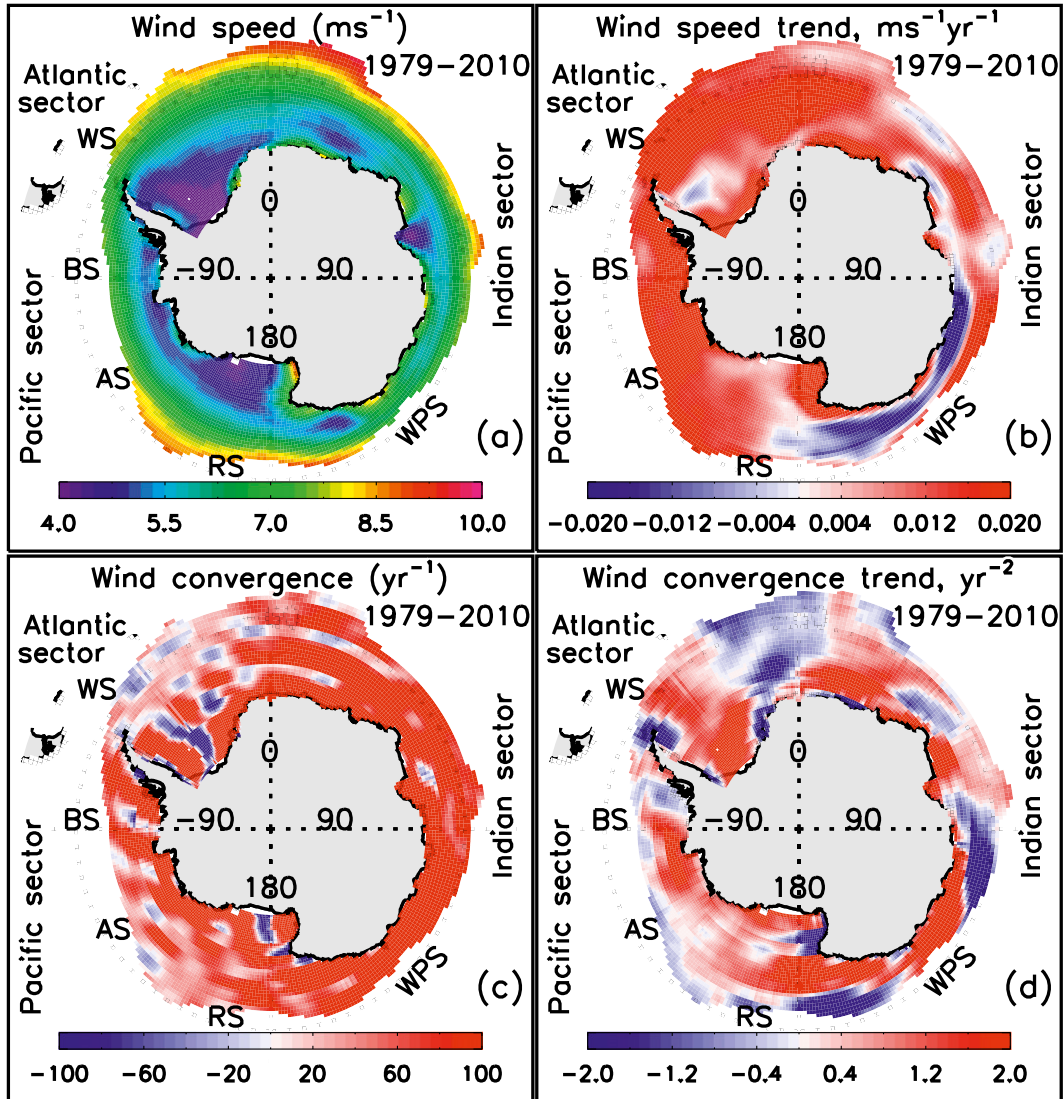


FIG. 1. Mean and linear trends of the NCEP–NCAR reanalysis (a),(b) surface wind speed and (c),(d) surface wind convergence (defined as $-\mathbf{V} \cdot \mathbf{u}_w$, where \mathbf{u}_w is surface wind velocity) over 1979–2010. WS, BS, AS, RS, and WPS represent the Weddell, Bellingshausen, Amundsen, and Ross Seas and the western Pacific sector, respectively.

indicator of climate change, which depends not only on ice area, but also on ice thickness. Ice extent has been well measured from space for the past 30 years using passive microwave instruments (e.g., Comiso and Nishio 2008; Parkinson and Cavalieri 2012). However, a long-term record of Antarctic sea ice volume is difficult to establish because of insufficient observations of ice thickness. Here, changes in Antarctic sea ice volume over 1979–2010 are estimated using a coupled global sea ice–ocean model driven by the National Centers for Environmental Prediction–National Center for Atmospheric Research (NCEP–NCAR) reanalysis atmospheric forcing data. Results of this model study may shed light on sea ice processes in response to changes in winds.

2. Model description

The coupled global sea ice–ocean model is based on the parallel ocean and sea ice model (POIM; Zhang and Rothrock 2003). Briefly, the global POIM couples the Parallel Ocean Program (POP) developed at the Los Alamos National Laboratory (e.g., Smith et al. 1992) with an eight-category thickness and enthalpy distribution (TED) sea ice model (Zhang and Rothrock 2003). The centers (upper limits) of the eight ice thickness categories are 0 (0.10), 0.38 (0.66), 1.30 (1.93), 3.07 (4.20), 5.97 (7.74), 10.24 (12.74), 16.02 (19.31), and 23.41 (27.51) m. The TED sea ice model explicitly simulates ice ridging processes following Thorndike et al. (1975)

TABLE 1. The 1979–2010 mean and linear trends for some variables of the NCEP–NCAR reanalysis data, model simulation results, and satellite observations based on the HadISST dataset. All variables except ice extent, volume, and ridged ice production are averaged over the ice-covered areas. Boldface numbers exceed the 95% confidence level when tested in a way that accounts for temporal autocorrelation.

	Mean	Trend	Trend/ Mean $\times 100\%$ (% yr ⁻¹)
Reanalysis surface wind speed	5.80 m s ⁻¹	0.0078 m s ⁻¹ yr ⁻¹	0.13
Reanalysis surface wind convergence	106.33 yr ⁻¹	0.70 yr ⁻²	0.66
Simulated ice speed	0.084 m s ⁻¹	7.9×10^{-5} m s ⁻¹ yr ⁻¹	0.094
Simulated ice strength	11 000 N m ⁻²	97.59 N m ⁻² yr ⁻¹	0.89
Simulated ice convergence	0.11 yr ⁻¹	0.0035 yr ⁻²	3.18
Simulated ridged ice production	2.98×10^{12} m ³ yr ⁻¹	0.032 $\times 10^{12}$ m ³ yr ⁻²	1.1
Simulated ice volume	15.15×10^{12} m ³	0.069 $\times 10^{12}$ m ³ yr ⁻¹	0.46
Simulated thick ice (>2 m) volume	6.69×10^{12} m ³	0.061 $\times 10^{12}$ m ³ yr ⁻¹	0.91
Simulated ice area fraction	0.64	0.0018 yr ⁻¹	0.28
Satellite observed ice area fraction	0.68	0.0016 yr ⁻¹	0.24
Simulated ice extent	12.73×10^{12} m ²	0.022 $\times 10^{12}$ m ² yr ⁻¹	0.17
Satellite observed ice extent	12.57×10^{12} m ²	0.027 $\times 10^{12}$ m ² yr ⁻¹	0.21

and Hibler (1980). Using the dynamics model of Zhang and Hibler (1997), sea ice motion is solved from a momentum equation that consists of a teardrop plastic rheology (Zhang and Rothrock 2005). Accompanying the TED sea ice model is an eight-category snow thickness distribution model. The snow conservation equation and the treatment of the snow thickness distribution are given by Flato and Hibler (1995, their appendix).

The global POIM grid configuration is based on a generalized orthogonal curvilinear coordinate system. In the Northern Hemisphere, the model grid is a gradually stretched curvilinear coordinate grid with the northern grid pole displaced into Greenland. In the Southern Hemisphere, the model grid is a regular spherical coordinate grid. The horizontal dimension is 360×276 with a resolution of $\langle 0.65^\circ \rangle$ (brackets denote the average resolution of surface ocean points).

The model is driven by the daily NCEP–NCAR reanalysis surface atmospheric forcing data over the period 1979–2010. The reanalysis forcing consists of 10-m surface winds, 2-m surface air temperature (SAT), specific humidity, precipitation, evaporation, sea level pressure, and cloud fraction. SAT and cloud fraction are used to calculate downwelling shortwave and longwave radiation following Parkinson and Washington (1979). More model details are found in Zhang (2007) and Zhang and Rothrock (2003).

In addition to the standard model integration mentioned above, a sensitivity run is conducted to further elucidate the effect of wind intensification on the sea ice cover. This sensitivity run is a model integration using the same reanalysis forcing except that the surface winds are from 1994, which is picked because it is at the middle of the study period 1979–2010. In the sensitivity run (denoted as Wind94 hereafter), the 1994 daily surface winds are used to drive the model repeatedly over the

whole period, thus removing any trends and interannual variability in the wind forcing.

The solution of the subgrid ice thickness distribution makes it possible to calculate the volume of ice in various thickness categories. For the purpose of analysis, we combine the various ice categories into three groups: thin ice (thickness ≤ 1 m), medium thick ice ($1 \text{ m} < \text{thickness} \leq 2$ m), and thick ice (thickness > 2 m). Thin ice thickness is hereafter defined as thin ice volume per unit area. Medium thick ice thickness or thick ice thickness is defined similarly. The combined volume per unit area of these three groups (or the summation of the thicknesses of these three groups) is defined hereafter as

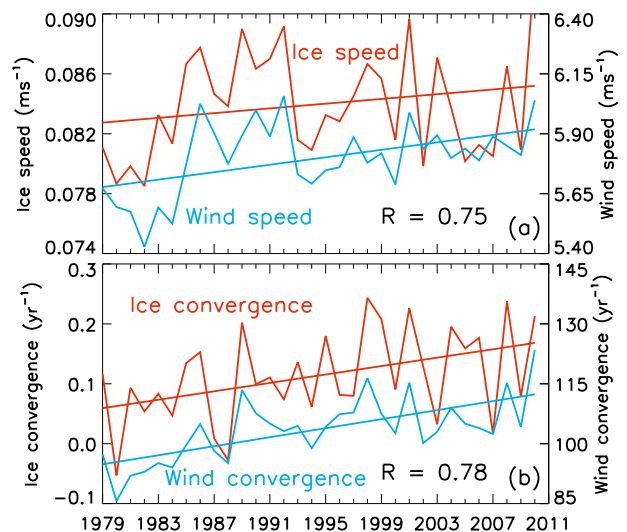


FIG. 2. Annual-mean NCEP–NCAR reanalysis (a) surface wind speed and model-simulated sea ice speed and (b) wind convergence and model-simulated ice convergence over the ice-covered areas of the Southern Ocean. Straight lines are trend lines. Correlation is listed in the lower right of (a) and (b).

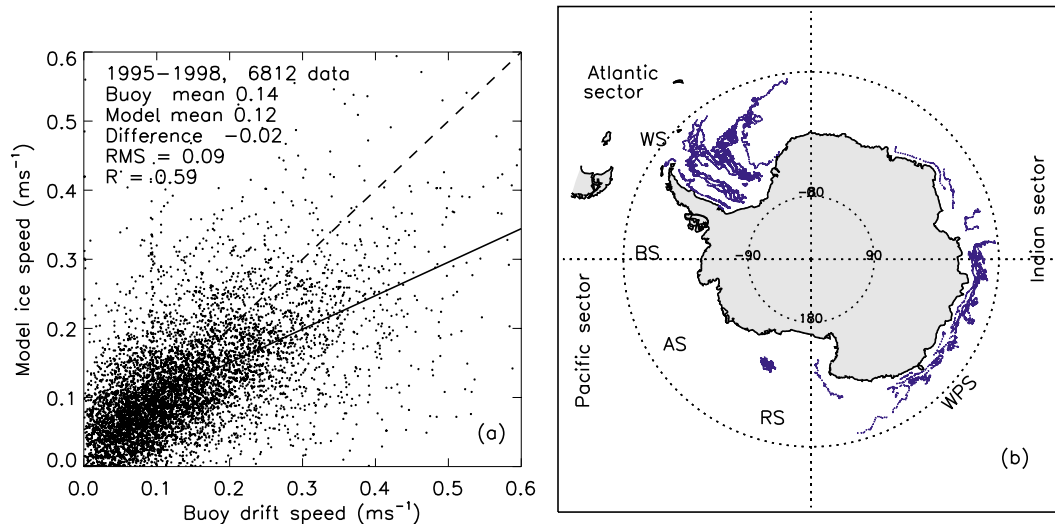


FIG. 3. (a) A comparison of daily buoy drift speeds and corresponding model results at the buoy locations. The black dots are individual buoy drift data (with 6812 data points) compared to model results. The buoy drift data are from the International Program for Antarctic Buoy, available online at the NSIDC website (http://nsidc.org/data/docs/daac/nsidc0084_ipab_antarctic_buoys.gd.html). They were collected during 1995–98 in the Indian Ocean and western Pacific sectors and the Weddell and Ross Seas with ice concentration at or above 40%. (b) The locations of these 6812 buoy drift velocities are shown by blue dots. In (a), the dashed line indicates equality and the solid line represents the best fit to the data. The overall buoy and model drift mean, model–data difference, root-mean-square (RMS) difference, and correlation are listed.

ice thickness, which can also be calculated by integrating the thickness distribution over the eight ice categories (Hibler 1980). Ice-covered areas in the Southern Ocean are defined as the 1979–2010 mean satellite observed sea ice extent (areas with ice concentration $\geq 15\%$); ice area fraction is defined as the mean ice concentration over whole ice-covered areas. Here, we present results over the period 1979–2010 when satellite sea ice concentration/extent data are available for analysis and model–data comparison. Results presented here are mainly from the standard simulation, unless stated otherwise.

3. Surface wind forcing

To ensure that the NCEP–NCAR reanalysis dataset is useful to explore the impact of wind intensification numerically, the properties of its surface wind forcing are examined for the period 1979–2010 over the SO ice-covered areas. The NCEP–NCAR reanalysis wind forcing shows wind intensification during the period. This is reflected in the spatial distribution of the linear surface wind speed (SWS) trends (Fig. 1b). Except for some areas of the Pacific and Indian Ocean sectors where SWS has decreased, an increase in SWS has occurred in most of the SO, according to the reanalysis data. Since 1979 the increase in SWS is $0.13\% \text{ yr}^{-1}$ averaged over the ice-covered areas of the SO (Table 1). This increase is significant at a 95% confidence level

tested using Fisher transformation (e.g., Devore 1995). However, the average wind speed shows considerable interannual variability (Fig. 2a).

In conjunction with an increase in SWS is a general increase in surface wind convergence (SWC, defined as $-\mathbf{V} \cdot \mathbf{u}_w$, where \mathbf{u}_w is surface wind velocity; Figs. 1d and 3b; Table 1). On average, SWC is mostly positive in the SO (Fig. 1c). It decreased in part of the Atlantic sector, but increased in most of the other sectors of the SO, particularly in the Weddell Sea and the Bellingshausen, Amundsen, and Ross (BAR) Seas (Fig. 1d). Over the ice-covered areas, the average SWC increase is $0.66\% \text{ yr}^{-1}$. Note that the rates of change in SWS and SWC may differ with other atmospheric reanalysis data or observations (Yuan 2004). However, the NCEP–NCAR reanalysis wind forcing, with increasing SWS and SWC, is ideal for numerical experiments to explore the impact of wind intensification on Antarctic sea ice volume.

4. Results

To realistically estimate sea ice response to wind intensification, the model needs to be able to simulate ice motion with some skill. To evaluate model performance in simulating ice motion, daily model ice speeds are compared with available buoy drift data from the International Programme for Antarctic Buoy (IPAB; Fig. 3a). The buoy drift data were collected during 1995

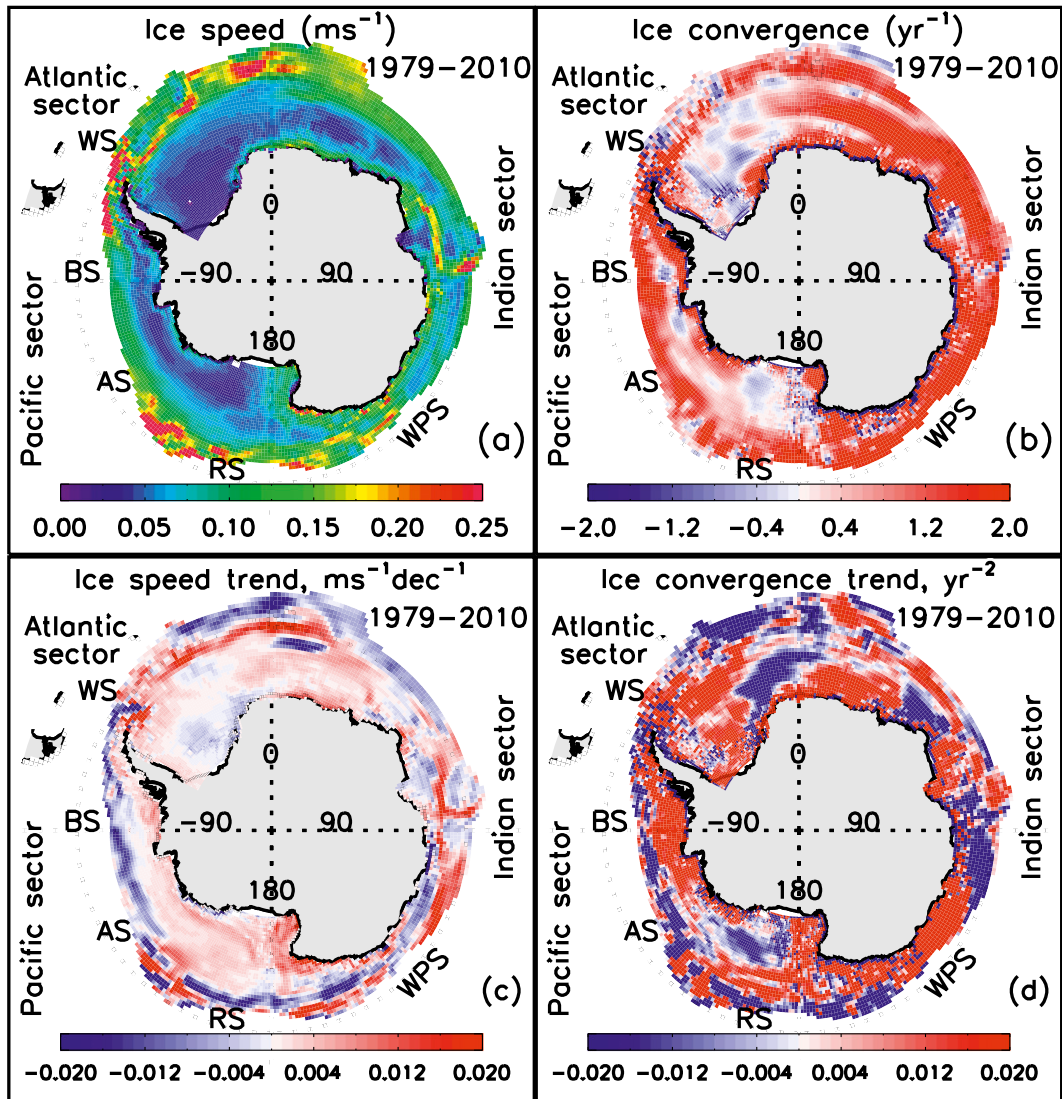


FIG. 4. Mean and linear trends of model-simulated (a),(c) sea ice speed and (b),(d) convergence over 1979–2010.

through 1998 in the Indian Ocean and western Pacific sectors and the Weddell and Ross Seas (Fig. 3b) and are available at the National Snow and Ice Data Center (NSIDC). The simulated daily ice speed is significantly correlated ($R = 0.59$) with the daily buoy drift speed (with 6812 data points), indicating that the model is able to capture 35% of the variance of the observations. On average, the model tends to underestimate ice motion represented by the buoy data. Part of the reason is that the model has fewer ice speeds that are larger than 0.4 m s^{-1} when compared to the point measurements of the buoys (Fig. 3a). However, the overall model bias is relatively low at -0.02 m s^{-1} or -14% .

Model-simulated ice motion is generally slower in most of the southern Weddell and BAR Seas compared with most of the northern parts of the SO (Fig. 4a). The

simulated ice speed increases in most of the SO during 1979–2010 in response to increasing SWS (Table 1; Figs. 2a and 4c). However, the increase in the average ice speed over the ice-covered areas of the SO, at 0.094 yr^{-1} , is relatively small, when compared to other variables in Table 1, and does not achieve the 95% confidence level. This is because the simulated ice volume (or ice thickness) increases (Table 1), which increases ice strength (Table 1) and tends to reduce ice motion through ice internal interaction described by the teardrop plastic rheology. Nevertheless, the interannual variability of the average ice speed is significantly correlated with that of SWS ($R = 0.75$; Fig. 2a).

Model-simulated sea ice convergence (defined as $-\mathbf{V} \cdot \mathbf{u}_i$, where \mathbf{u}_i is ice velocity) also increases in response to increasing SWC (Table 1; Fig. 2b). Like SWC (Fig. 1c),

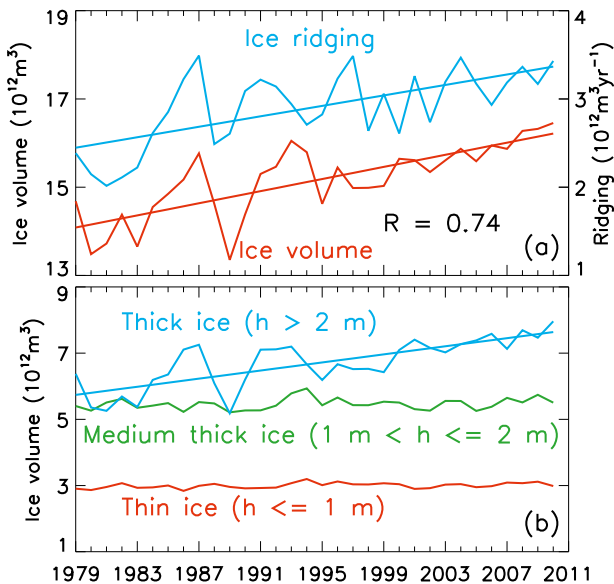


FIG. 5. Annual-mean model-simulated (a) total ridged ice production and ice volume and (b) total volumes of thin ice, medium thick ice, and thick ice in the Southern Ocean. Correlation is listed in the lower right of (a).

ice convergence on average is mostly positive in the SO (Fig. 4b). The spatial pattern of linear trends of ice convergence over 1979–2010 (Fig. 4d) is also similar to that of SWC (Fig. 1d), with mostly positive values. Overall, the average ice convergence increases by $3.18\% \text{ yr}^{-1}$, much higher than the increase in ice speed and exceeding the 95% confidence level. This is because ice convergence is influenced by increases of both SWS and SWC. The average ice convergence is significantly correlated with SWC ($R = 0.78$; Fig. 2b).

The increase in ice convergence (as well as shear deformation rate, not shown) drives an increase in total ridged ice production in the SO (Table 1; Fig. 5a). This is because convergence and shear deformation have a role in ice ridging (Thorndike et al. 1975). The simulated ridged ice production is significant in all months except January–March and December (Fig. 6). It peaks during July–September. Spatially, ice ridging occurs mostly in the Weddell and BAR Seas (Fig. 7a) where ice is generally thicker than in other areas of the SO (Fig. 7b). The mean annual ridged ice production in the coastal Weddell and BAR Seas can be as high as 1.5 m. As ice convergence increases in response to increasing SWS and SWC in these regions, ridged ice production increases (Fig. 7c). Spatially, the correlation between ridged ice production and ice convergence is mostly positive in the Weddell and BAR Seas (Fig. 8a), as is the correlation between ridged ice production and SWC (Fig. 8b). The correlation between the average ice convergence and

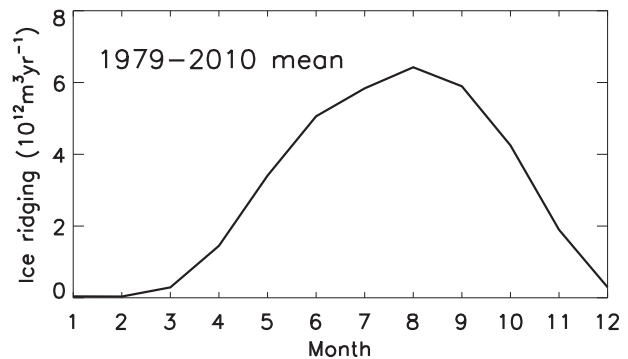


FIG. 6. Model-simulated seasonal cycle of 1979–2010 mean total ridged ice production in the Southern Ocean.

ridged ice production is 0.78 for the whole Weddell Sea and 0.57 for the BAR Seas.

In conjunction with increased ridged ice production is increased ice thickness (Fig. 7d). This is expected because increased ridging transforms more thin ice into thick ice mechanically, which tends to increase the area of open water and hence enhance winter ice growth, leading to an increase in ice thickness. An increase in ice thickness also tends to allow more ice to participate in ridging, leading to an increase in ridging production (Hibler 1980). The correlation between ice thickness and ridged ice production is mostly positive in the Weddell and BAR Seas (not shown), as is the correlation between ice thickness and wind convergence (Fig. 8c). The increase in ice thickness in these regions leads to an increase in the simulated total ice volume in the SO (Fig. 5a; Table 1). The total ice volume is correlated ($R = 0.74$) significantly with ridged ice production, which is in turn correlated with SWS and SWC ($R = 0.79$ and 0.66 , respectively; Table 2). The total ice volume is correlated with SWS and SWC to a lesser degree.

The simulated total ice volume is most highly correlated with the total thick ice volume ($R = 0.96$; Table 2), indicating that changes in ice mass are dominated by changes in thick ice in the SO. Thick ice (Fig. 9a) is mostly concentrated in the Weddell and BAR Seas, while medium thick ice (Fig. 9b) and thin ice (not shown) are often found in all sectors of the SO (Worby et al. 2008). The spatial pattern of thick ice thickness trends (Fig. 9c) largely resembles the spatial patterns of ridged ice production (Fig. 7c) and ice thickness (Fig. 7d). This is why the spatial pattern of correlation between thick ice thickness and SWC (Fig. 8d) is similar to that between ice thickness and SWC (Fig. 8c). In the Weddell and BAR Seas in particular, the increase in ice thickness is mainly due to a similar increase in thick ice. Trends in the volume per unit area of medium thick ice (and thin ice, not shown) are much smaller than those of

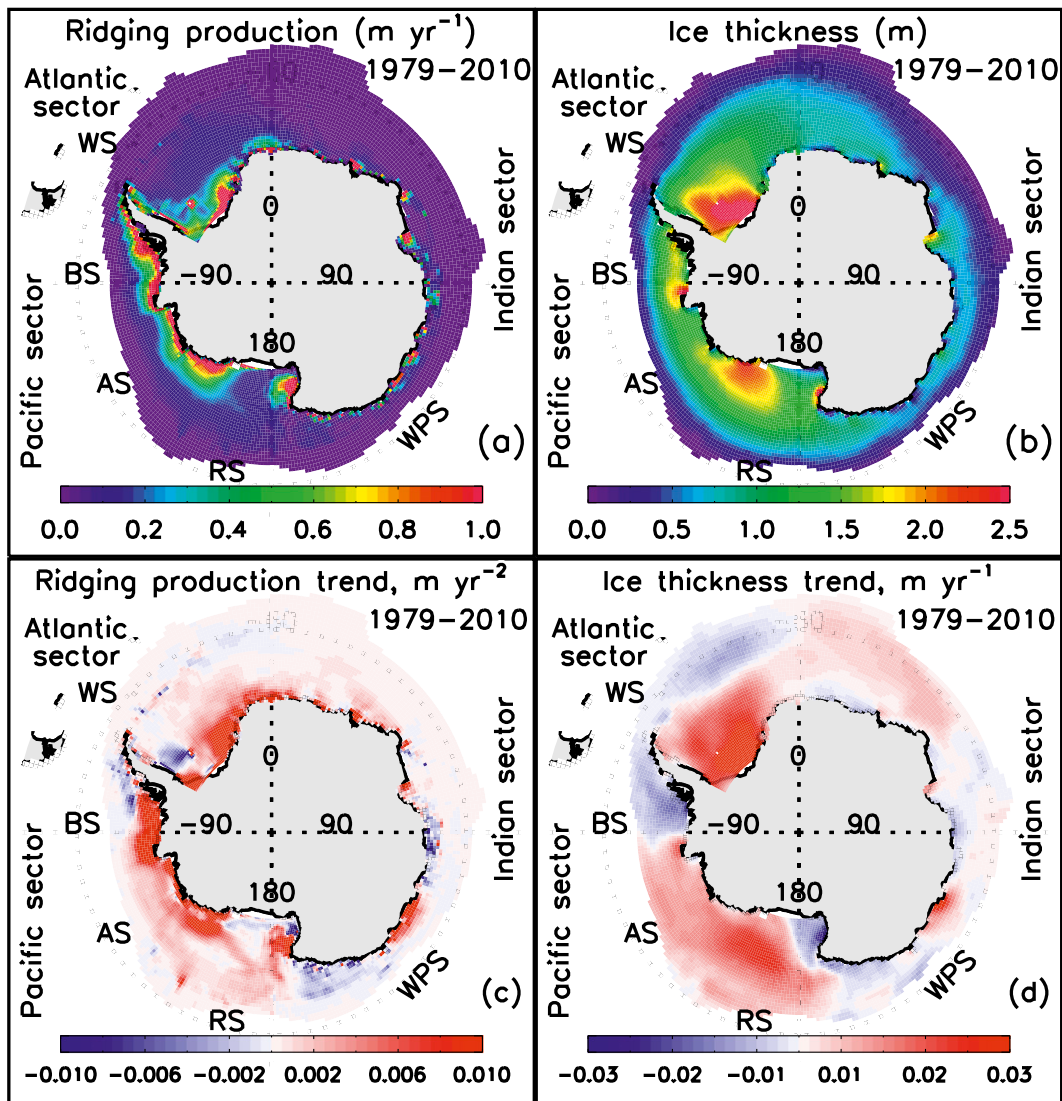


FIG. 7. Mean and linear trends of model-simulated (a),(c) ridged ice production and (b),(d) ice thickness over 1979–2010.

thick ice (Fig. 9d). The total volumes of medium thick ice and thin ice in the SO remain unchanged during 1979–2010, while the total volume of thick ice increases significantly (Fig. 5b; Table 1). This reflects the increased mechanical redistribution of the ice mass from thin ice to thick ice, owing to increased ridging in response to wind intensification. Nevertheless, even with increased mechanical transfer of thin ice into thick ice, the simulated total volumes of thin ice and medium thick ice in the SO seldom decrease during 1979–2010. This is because increased ice ridging tends to increase the open water fraction and hence enhance winter growth of often thin and medium thick ice. The total thick ice volume in the SO is correlated, to a varying degree, with ridging production, SWS, and SWC (Table 2), while no significant

correlation is found with the total medium thick ice volume (Table 2) or with the total thin ice volume (not shown).

The areas of more thick ice, mainly in the Weddell and BAR Seas, are characterized by higher ice concentration (Figs. 10a,b). The model over- or underestimates ice concentration in some areas such as in the Weddell Sea, but captures the observed spatial pattern with more compact ice in the Weddell and BAR Seas and less compact ice elsewhere (Figs. 10a,b). Both satellite observations and model results show an increasing Antarctic sea ice cover since 1979, characterized by an increasing ice area fraction and ice extent (Table 1; Figs. 11a,b). The satellite observed increase in the ice cover is caused by a significant increase in ice concentration in most of the Indian Ocean sector and parts of

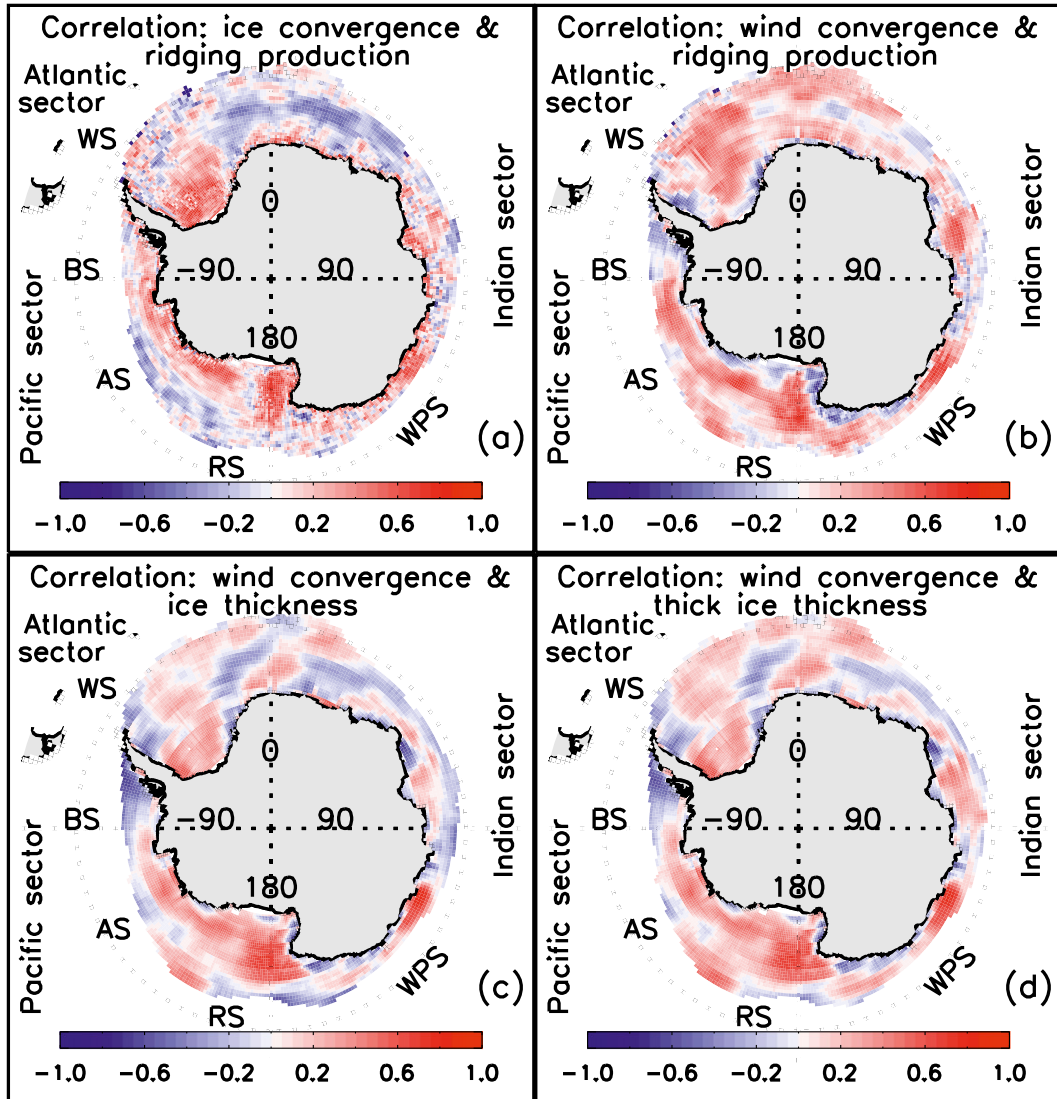


FIG. 8. Spatial distribution of correlation (a) between the simulated ice convergence and ridged ice production, (b) between reanalysis wind convergence and simulated ridged ice production, (c) between wind convergence and simulated ice thickness, and (d) between wind convergence and simulated thick ice volume per unit area over the ice-covered areas of the Southern Ocean.

the Atlantic and Pacific sectors, including areas in the Weddell and Ross Seas (Fig. 10d). However, ice concentration decreased considerably in some areas in the Atlantic and Pacific sectors, particularly in the Bellingshausen Sea where atmospheric warming is the strongest (e.g., Vaughan et al. 2003). This asymmetry of Antarctic sea ice cover increase/decrease yields an observed modest overall increase in ice extent ($0.21\% \text{ yr}^{-1}$) and in ice area fraction ($0.24\% \text{ yr}^{-1}$; Table 1). The observed trends are derived based on the Hadley Centre Sea Ice and Sea Surface Temperature dataset (HadISST; <http://badc.nerc.ac.uk/browse/badc/ukmo-hadisst>). The derived trends based on the HadISST dataset may be exaggerated

somewhat because of a sudden increase in ice concentrations in the central ice pack in 2009, which is as a result of a switch in the data sources from the Special Sensor Microwave Imager (SSM/I) to the Advanced Microwave Scanning Radiometer for the Earth Observing System (AMSR-E; Screen 2011). Trends may also differ if calculated from different datasets because of different algorithms and sensors (Comiso and Nishio 2008); for example, the observed ice extent trend during the period 1978–2010 is estimated to be $0.14 \pm 0.02\% \text{ yr}^{-1}$ by J. Comiso (2011, personal communication).

In comparison, the model simulates an increase of $0.17\% \text{ yr}^{-1}$ in ice extent and an increase of $0.28\% \text{ yr}^{-1}$ in

TABLE 2. Correlations among annual-mean model-simulated total ridged ice production (RIP), ice volume (IV), thick ice volume (TIV), and medium thick ice volume (MIV) and NCEP–NCAR reanalysis SWS and SWC over the period 1979–2010. Boldface numbers exceed the 95% confidence level.

	IV	TIV	MIV	SWS	SWC
RIP	0.74	0.78	0.08	0.79	0.66
IV		0.96	0.46	0.45	0.49
TIV			0.19	0.58	0.54
MIV				−0.26	−0.06
SWS					0.67

ice area fraction (Table 1). The model captures the observed ice concentration trends in most areas, particularly in the Weddell Sea and the Indian Ocean and western Pacific sectors (Figs. 10c,d). However, model

discrepancies exist in some areas of the southern Amundsen (southwestern Ross) Sea where the model has increasing (decreasing) trends while satellite data show decreasing (increasing) trends. Overall, the simulated ice area fraction and extent are correlated to the corresponding observations with similar increasing trends ($R = 0.74$ and 0.62 , respectively; Figs. 11a,b; Table 1). However, the increasing trends of either observed or simulated ice area fraction and ice extent are significantly smaller than those of simulated thick ice volume and hence total ice volume, indicating the significant impact of wind intensification on the variability and trends of ice volume through ridging processes.

Finally, we examine the results from the sensitivity run Wind94. Unlike the standard model run, Wind94 does not simulate a positive trend in either ice speed or

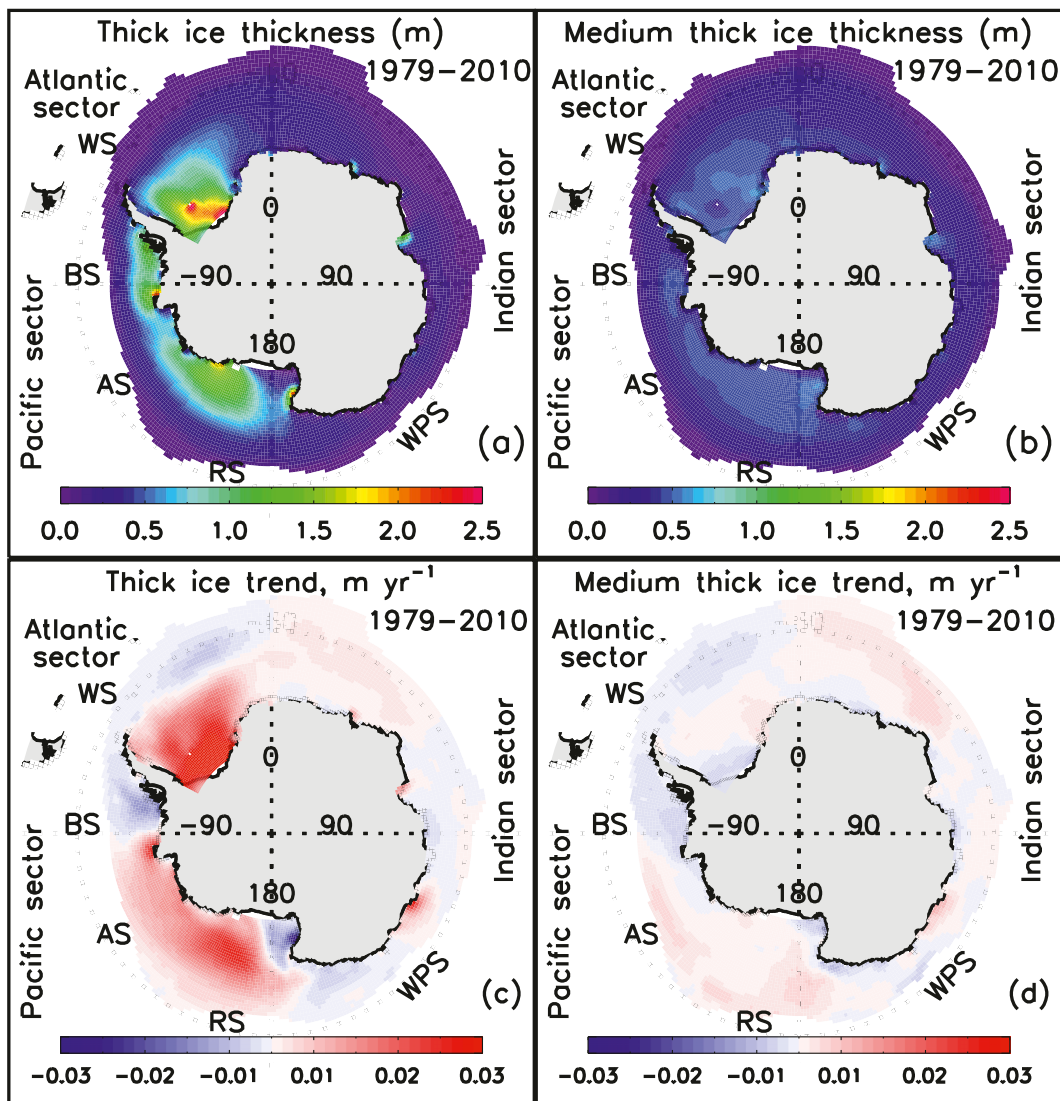


FIG. 9. Mean and linear trends of model-simulated (a),(c) thick ice volume per unit area and (b),(d) medium thick ice volume per unit area over 1979–2010. Here, thick ice volume per unit area and medium thick ice volume per unit area are referred to as thick ice thickness and medium thick ice thickness.

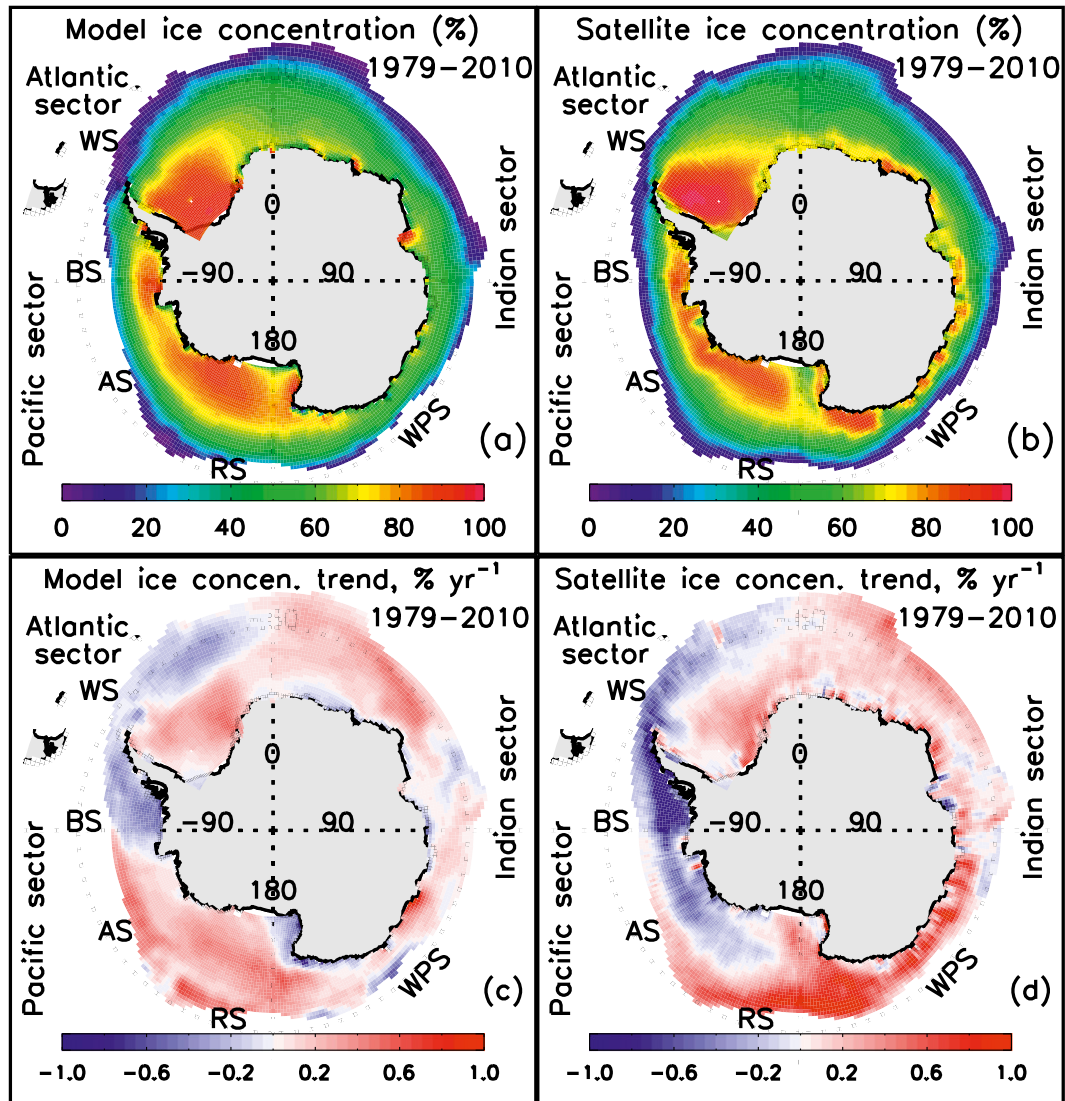


FIG. 10. Mean and linear trends of (a),(c) model-simulated ice concentration and (b),(d) satellite-observed ice concentration over 1979–2010.

ice convergence (Fig. 12a). This is expected because the 1994 wind forcing is applied repeatedly in the sensitivity simulation. In fact, the simulated ice speed and convergence both show a tendency to decrease over 1979–2010. This is linked to Wind94's simulation of an increase in ice volume (Fig. 12b) and hence ice strength, which tends to reduce ice motion through stronger ice internal interaction, as mentioned earlier. The decrease in ice speed and convergence leads to a decrease in ice ridging (Fig. 12b). As a result, the increase in ice volume (Fig. 12b) or thick ice volume (Fig. 12c) is significantly smaller than the increase with the standard simulation, further illustrating the role of wind intensification in boosting ridged ice production and hence ice volume.

5. Concluding remarks

Satellite passive microwave images and some model simulations of Antarctic sea ice cover show an overall increase in ice area fraction, extent, and volume (e.g., Parkinson and Cavalieri 2012; Zhang 2007; Table 1; Figs. 5 and 11) despite evidence of generally warming atmospheric and oceanic conditions in the Antarctic region (e.g., Turner et al. 2006; Gille 2008). However, there is also a strong asymmetry in sea ice cover changes, with significant ice decline in some areas such as the Bellingshausen Sea and ice expansion in some other areas (Figs. 7b and 10c,d). The strong asymmetry in sea ice changes is certainly linked to the fact that Antarctic SAT

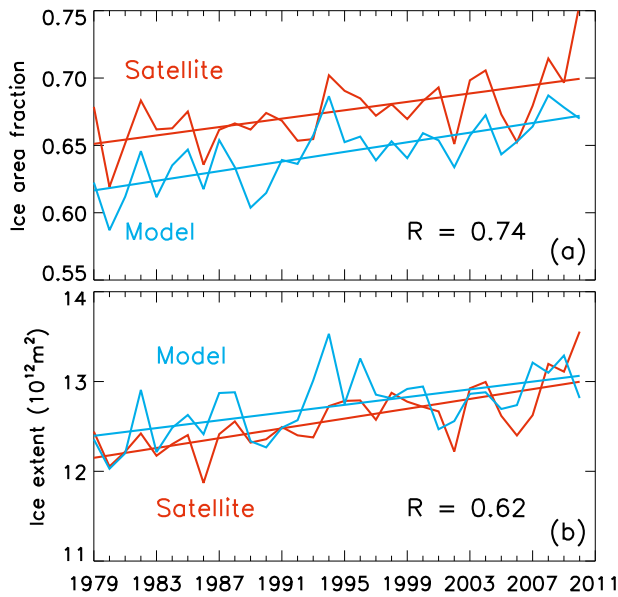


FIG. 11. Annual-mean (a) satellite-observed and model-simulated ice area fraction over the ice-covered areas and (b) satellite-observed and model-simulated ice extent of the Southern Ocean. Correlation is listed in the lower right of (a) and (b).

variability is complicated, and long-term trends vary greatly depending on location and season (Vaughan et al. 2003; Monaghan et al. 2008).

The complex variability and trend patterns of Antarctic sea ice cover are also linked to changes in the southern annular mode (SAM) and El Niño–Southern Oscillation (e.g., Yuan and Martinson 2000; Kwok and Comiso 2002; Liu et al. 2004; Stammerjohn et al. 2008). Particularly, the SAM has shifted to more positive phases over recent decades (e.g., Kidson 1999; Marshall 2003), which may be linked to ozone depletion and greenhouse gas increases (Thompson and Solomon 2002; Shindell and Schmidt 2004). The SAM shift is associated with wind intensification (Hurrell and van Loon 1994; Thompson and Solomon 2002) and changes in ocean circulation (Hall and Visbeck 2002) that may affect the variability of the sea ice cover. Here, the impact of wind intensification on Antarctic sea ice volume is investigated using a numerical model driven by the NCEP–NCAR reanalysis forcing with generally increasing SWS and SWC.

As mentioned, the increasing rates of SWS and SWC derived from the NCEP–NCAR reanalysis may differ with other atmospheric reanalysis data or observations (Yuan 2004). The NCEP–NCAR reanalysis underestimates the SO surface wind strength in high wind bands, when compared to Quick Scatterometer (QuikSCAT) and weather station data (Yuan 2004). This suggests that the dataset may have a tendency to underestimate the

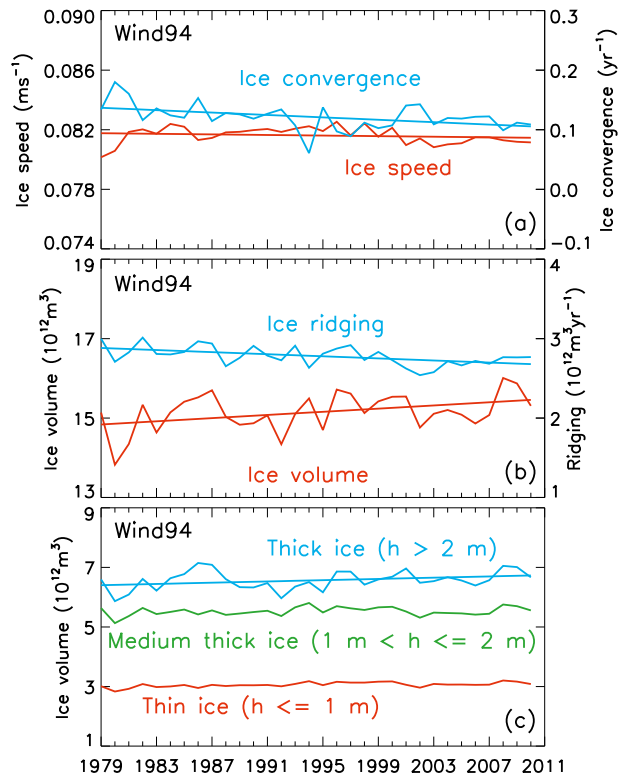


FIG. 12. Annual-mean (a) sea ice speed and convergence over the ice-covered areas of the Southern Ocean, (b) total ridged ice production and ice volume, and (c) total volumes of thin ice, medium thick ice, and thick ice in the Southern Ocean, simulated by the Wind94 case.

intensification of the winds in high wind bands. On the other hand, Marshall (2003) reports that the positive trend in the SAM index derived from the NCEP–NCAR reanalysis is larger than a reconstruction from station data and the 40-yr European Centre for Medium-Range Weather Forecasts (ECMWF) Re-Analysis (ERA-40). Although there are various SAM definitions and indices with similarities and discrepancies (Ho et al. 2012), the Marshall (2003) study indicates that the NCEP–NCAR reanalysis data may overestimate wind intensification and hence the rates of change in SWS and SWC. Thus, there are uncertainties in the magnitude of the SO wind intensification in the NCEP–NCAR reanalysis forcing, suggesting that much work needs to be done in SO reanalyses so that future sea ice thickness changes may be accurately reflected in climate models using reanalysis forcing.

Despite the uncertainties in the NCEP–NCAR reanalysis forcing, the model is able to capture 35% of the variance of daily buoy drift speed with a relatively low overall bias for the period of available buoy data, 1995–98. It also captures reasonably well the interannual variability and trends of the Antarctic sea ice area fraction

and extent over the period 1979–2010. Model results indicate that the wind intensification tends to cause an increase in the model-simulated ice speed, convergence, and shear deformation rate, leading to an increase in the simulated ridged ice production, mainly in the Weddell and BAR Seas where the increase in wind convergence dominates. In the southern Weddell Sea, the increase in ridging and hence ice thickness may be a contributing factor to the observed increase in ice concentration there. Over the whole SO, the increase in ice ridging leads to an increase in the simulated thick ice volume and hence the total ice volume. The thin ice and medium thick ice volumes remain unchanged over the past three decades, even though more thin ice is transferred to thick ice through mechanical redistribution. The percentage increase in the total ice volume, and particularly the thick ice volume, is much higher than the percentage increase in other sea ice parameters such as ice area fraction and extent, observed or simulated, suggesting that the wind intensification has a greater impact on the changes in ice volume. The higher increase in ice volume may also suggest that ice volume is a potentially strong measure of change.

The Wind94-simulated increase in ice volume is less than the standard model run. Nevertheless, the result from Wind94 suggests that factors other than winds may have a role in the modest increase in ice volume. A prior model study (Zhang 2007) reports that changes in thermodynamic processes may contribute to increasing Antarctic sea ice under generally warming atmospheric and oceanic conditions. An increase in SAT results in an increase in the upper-ocean temperature and a decrease in sea ice freezing.

A decrease in ice freezing in turn leads to a decrease in salt rejection from ice in the upper-ocean salinity and in the upper-ocean density. The enhanced ocean stratification tends to suppress convective overturning, leading to a decrease in the upward ocean heat flux available to melt ice. Net melting decreases faster than net freezing, resulting in an increase in net ice production. This mechanism (Zhang 2007) may be useful to explain the slight increase in ice volume with the Wind94 sensitivity simulation. The role of wind intensification is to further increase ice volume, as shown by the standard model run.

Acknowledgments. This work was supported by the National Science Foundation Office of Polar Programs (Grant ANT-0838769). The author thanks Dr. J. Comiso for providing the satellite observed ice extent trend and Dr. R. Kwok and three anonymous reviewers for constructive comments. The buoy drift data are from the International Programme for Antarctic Buoys, available

at the NSIDC, and the satellite ice concentration data are from the Met Office Hadley Centre.

REFERENCES

- Comiso, J. C., and F. Nishio, 2008: Trends in the sea ice cover using enhanced and compatible AMSR-E, SSM/I, and SMMR data. *J. Geophys. Res.*, **113**, C02S07, doi:10.1029/2007JC004257.
- Devore, J. L., 1995: *Probability and Statistics for Engineering and the Sciences*. Brooks/Cole Publishing Company, 743 pp.
- Flato, G. M., and W. D. Hibler III, 1995: Ridging and strength in modeling the thickness distribution of Arctic sea ice. *J. Geophys. Res.*, **100** (C9), 18 611–18 626.
- Fyfe, J., and O. Saenko, 2006: Simulated changes in the extratropical Southern Hemisphere winds and currents. *Geophys. Res. Lett.*, **33**, L06701, doi:10.1029/2005GL025332.
- Gille, S. T., 2008: Decadal-scale temperature trends in the Southern Hemisphere ocean. *J. Climate*, **21**, 4749–4765.
- Hall, A., and M. Visbeck, 2002: Synchronous variability in the Southern Hemisphere atmosphere, sea ice, and ocean resulting from the annular mode. *J. Climate*, **15**, 3043–3057.
- Hibler, W. D., III, 1980: Modeling a variable thickness sea ice cover. *Mon. Wea. Rev.*, **108**, 1943–1973.
- Ho, M., A. S. Kiem, and D. C. Verdon-Kidd, 2012: The southern annular mode: A comparison of indices. *Hydrol. Earth Syst. Sci.*, **16**, 967–982.
- Hurrell, J. W., and H. van Loon, 1994: A modulation of the atmospheric annual cycle in the Southern Hemisphere. *Tellus*, **46A**, 325–338.
- Kidson, J. W., 1999: Principal modes of Southern Hemisphere low-frequency variability obtained from NCEP–NCAR reanalyses. *J. Climate*, **12**, 2808–2830.
- Kwok, R., and J. C. Comiso, 2002: Spatial patterns of variability in Antarctic surface temperature: Connections to the Southern Hemisphere annular mode and the Southern Oscillation. *Geophys. Res. Lett.*, **29**, doi:10.1029/2002GL015415.
- Liu, J., J. A. Curry, and D. G. Martinson, 2004: Interpretation of recent Antarctic sea ice variability. *Geophys. Res. Lett.*, **31**, L02205, doi:10.1029/2003GL018732.
- Marshall, G. J., 2003: Trends in the southern annular mode from observations and reanalyses. *J. Climate*, **16**, 4134–4143.
- Monaghan, A. J., D. H. Bromwich, W. Chapman, and J. C. Comiso, 2008: Recent variability and trends of Antarctic near-surface temperature. *J. Geophys. Res.*, **113**, D04105, doi:10.1029/2007JD009094.
- Parkinson, C. L., and W. M. Washington, 1979: A large-scale numerical model of sea ice. *J. Geophys. Res.*, **84** (C1), 311–337.
- , and D. J. Cavalieri, 2012: Antarctic sea ice variability and trends, 1979–2010. *Cryosphere*, **6**, 871–880, doi:10.5194/tc-6-871-2012.
- Screen, J. A., 2011: Sudden increase in Antarctic sea ice: Fact or artifact? *Geophys. Res. Lett.*, **38**, L13702, doi:10.1029/2011GL047553.
- Shindell, D. T., and G. A. Schmidt, 2004: Southern Hemisphere climate response to ozone changes and greenhouse gas increases. *Adv. Space Res.*, **33**, 1058–1061.
- Smith, R. D., J. K. Dukowicz, and R. C. Malone, 1992: Parallel ocean general circulation modeling. *Physica D*, **60**, 38–61.
- Spence, J. P., J. C. Fyfe, A. Montenegro, and A. J. Weaver, 2010: Southern Ocean response to strengthening winds in an eddy-permitting global climate model. *J. Climate*, **23**, 5332–5343.

- Stammerjohn, S. E., D. G. Martinson, R. C. Smith, and X. Yuan, 2008: Trends in Antarctic annual sea ice retreat and advance and their relation to El Niño–Southern Oscillation and southern annular mode variability. *J. Geophys. Res.*, **113**, C03S90, doi:10.1029/2007JC004269.
- Thompson, D., and S. Solomon, 2002: Interpretation of recent Southern Hemisphere climate change. *Science*, **296**, 895–899.
- Thorndike, A. S., D. A. Rothrock, G. A. Maykut, and R. Colony, 1975: The thickness distribution of sea ice. *J. Geophys. Res.*, **80** (33), 4501–4513.
- Turner, J., T. A. Lachlan-Cope, S. Colwell, G. J. Marshall, and W. M. Connolley, 2006: Significant warming of the Antarctic winter troposphere. *Science*, **311**, 1914–1917.
- Vaughan, D. G., and Coauthors, 2003: Recent rapid regional climate warming on the Antarctic Peninsula. *Climatic Change*, **60**, 243–274.
- Worby, A. P., C. A. Geiger, M. J. Paget, M. L. Van Woert, S. F. Ackley, and T. L. DeLiberty, 2008: Thickness distribution of Antarctic sea ice. *J. Geophys. Res.*, **113**, C05S92, doi:10.1029/2007JC004254.
- Yuan, X., 2004: High wind evaluation in the Southern Ocean. *J. Geophys. Res.*, **109**, D13101, doi:10.1029/2003JD004179.
- , and D. G. Martinson, 2000: Antarctic sea ice extent variability and its global connectivity. *J. Climate*, **13**, 1697–1717.
- Zhang, J., 2007: Increasing Antarctic sea ice under warming atmospheric and oceanic conditions. *J. Climate*, **20**, 2515–2529.
- , and W. D. Hibler III, 1997: On an efficient numerical method for modeling sea ice dynamics. *J. Geophys. Res.*, **102** (C4), 8691–8702.
- , and D. A. Rothrock, 2003: Modeling global sea ice with a thickness and enthalpy distribution model in generalized curvilinear coordinates. *Mon. Wea. Rev.*, **131**, 681–697.
- , and —, 2005: The effect of sea ice rheology in numerical investigations of climate. *J. Geophys. Res.*, **110**, C08014, doi:10.1029/2004JC002599.